Process Fundamentals of Membrane Emulsification: Simulation with CFD

A. J. Abrahamse, A. van der Padt, and R. M. Boom
Food and Bioprocess Engineering Group, Wageningen University, P.O. Box 8129, 6700 EV Wageningen, The Netherlands

W. B. C. de Heij
ATO, Preservation Technology and Food Safety, P.O. Box 17, 6700 AA Wageningen, The Netherlands

Membrane emulsification is a process in which a to-be-dispersed phase is pressed through a membrane; the droplets formed are carried away with the continuous phase. To design a suitable membrane setup, more insight into the formation of the droplets at the membrane surface is needed. Therefore, the formation of one droplet from a cylindrical pore was calculated using computational fluid dynamics. From the resulting droplet diameter (33 μm; pore diameter, 5 μm) and the calculated droplet shape, the maximum membrane porosity was calculated to be 1.5%, to prevent coalescence of droplets growing on neighboring pores. Due to the deformation of the droplet and the formation of the neck, the pressure drop over the pore and the velocity of oil in the pore varied in time. During necking, the velocity in the pore decreased sharply. After detachment of the first droplet, no satellite droplets were formed, but a small oil volume remained attached at the pore, forming a new droplet.

Introduction

Emulsification is an important structure-forming process applied in the food, pharmaceutical, and cosmetics industry. A relatively new technique to produce emulsions is membrane emulsification: a process in which a to-be-dispersed phase is pressed through a membrane and droplets formed at the membrane surface are carried away with the continuous phase flowing across the membrane. Compared to other emulsification processes, this technique presents several advantages: low energy consumption, because only small shear stresses are needed to form the droplets; control of droplet size and droplet-size distribution; and easy scalability of the process. (Schröder and Schubert, 1999; Joscelyne and Trägårdh, 1999; Peng and Williams, 1998). Thus, with this process, food, cosmetic, and pharmaceutical emulsions can be improved and new products can be developed.

Until now, membrane emulsification has been studied with ceramic (Schröder et al., 1998; Joscelyne and Trägårdh, 1999) or glass tubular membranes (Omi, 1995). Originally these membranes were developed for separation purposes. Therefore, they are not necessarily optimal for emulsification. For example, their high porosity may increase coalescence of growing droplets at the membrane surface, which would enlarge the average droplet size and would render the emulsion more heterodisperse. In a different system, in which the droplet formation was visualized by microscopy, a well-defined emulsion was made (Kawakatsu et al., 1997). However, scale-up of this research system will not be a trivial task. Altogether, a scalable membrane system, tailor-made for membrane emulsification, will make this process commercially more viable.

To make a better design possible, insight into the process of droplet formation at the membrane surface is required. Recently, the important parameters determining the droplet size were identified by calculating the overall forces that act on the forming droplets (Schröder et al., 1998; Peng and Williams, 1998). Assuming a rigid, spherical droplet, the droplet size is determined by the cross-flow velocity of the continuous phase, the pore diameter, the transmembrane pressure, and the (dynamic) interfacial tension. In the two aforementioned studies the authors recognized that the droplet will be deformed because the acting forces have several directions, but the effect of this deformation on the final droplet size was not taken into account. To design an optimal

Correspondence concerning this article should be addressed to A. J. Abrahamse.

Table 1. Values of the Physical Properties and Constants used in the Simulation

Property	Value
Water density	1,000 kg·m^{-3}
Oil density	773 kg ·m^{-3}
Water viscosity	1×10^{-3} Pa·s
Oil viscosity	3×10^{-3} Pa·s
Interfacial tension	30 mN·m^{-1}
Wall contact angle for water	0°
Gravitational constant	9.81 m·s^{-2}

membrane for emulsification, it is important to know the shape of the droplets during their formation. The shape will determine, for instance, whether droplets coalesce at a given membrane surface. However, this shape cannot be calculated using overall (global) force equations. The shape changes locally due to variations in viscous and inertial forces. For example, the greater the distance from the membrane, the higher is the velocity of the continuous phase. As a result, local forces on the droplet vary in place and time, resulting in a changing droplet shape. Of course, this shape also depends on the values of other parameters such as dynamic interfacial tension and transmembrane pressure.

We calculated the shape of an oil droplet forming at a single cylindrical pore with computational fluid dynamics (CFD). In this article we describe the effect of droplet shape on the maximum porosity of the emulsification membrane and on the oil flux through the pore.

Model Set-up

The CFD software package used in this research was CFX 4.2 (AEA Technology, UK), which is a finite-volume code. The droplet formation was modeled as a 3-dimensional, multiphase system with laminar flow. Oil flowed through a cylindrical pore and water through a rectangular flow channel. The physical properties and constants are given in Table 1.

Geometry

The cylindrical pore had a diameter and a length of 5 μm. Only half of the height of the rectangular flow channel was modeled, since the flow is assumed to be symmetrical in the center plane of the channel ($z = 50$ μm; Figure 1a and 1b). The plane $y = 0$ was a symmetry plane as well (Figure 1a and 1c). The part of the flow channel that was modeled had a height of 50 μm (z-direction), a width of 37.5 μm (y-direction), and a length of 87.5 μm (x-direction).

Since it was expected that the velocities of both phases and the pressure change fastest at the outflow of the pore into the flow channel, the grid was made finest in that region. The pore was divided into 5520 control volumes, whereas the flow channel contained 156,120 control volumes (Figure 2). The smallest volume cell, which is approximately 1.5×10^{-20} m^3, contains about $3\cdot10^7$ oil molecules. This number is sufficient to consider the fluid as a continuum, hence the fluid can be described adequately with macroscopic properties such as velocity, pressure, and density.

Boundary conditions

Water flowed through the inlet of the flow channel in the x-direction with an average velocity of 0.5 m/s. A laminar

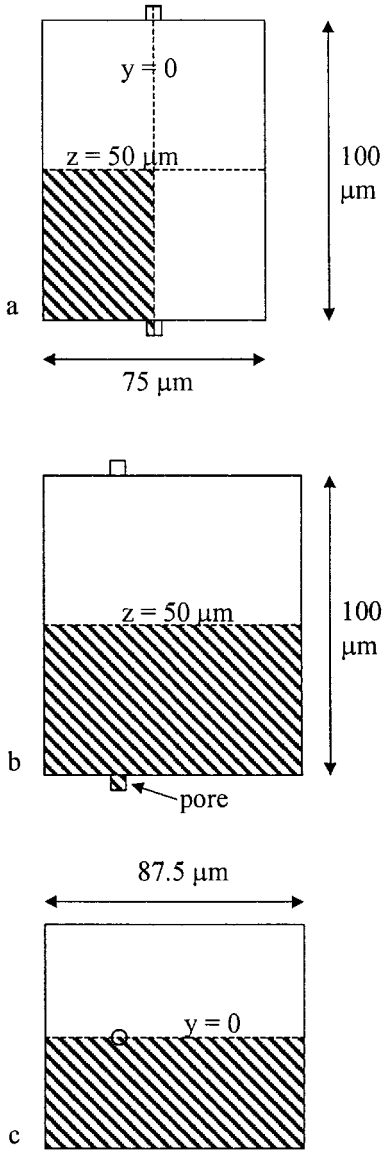

Figure 1. Rectangular flow channel and cylindrical pore.

The modeled geometry is depicted by the hatched planes; the symmetry planes are represented by dashed lines. (a) Side view (y-z plane); (b) front view (x-z plane); (c) bottom view (x-y plane).

(parabolic) velocity profile at the inlet was generated. At the outlet of the flow channel the pressure was set at 1.0×10^5 Pa. At the inlet of the pore the pressure was set at 1.3×10^5 Pa. The other geometry boundaries were walls, except for the symmetry planes ($y = 0$ and $z = 50$ μm). We assumed the no-slip condition to be valid at the walls, which means a local fluid velocity of 0 m/s at the walls.

Initial conditions

The initial conditions were programmed in Fortran. At $t = 0$ s the flow channel was filled with laminary flowing water and the pore was completely filled with oil. At $t = 0$ s the interface between oil and water was flat.

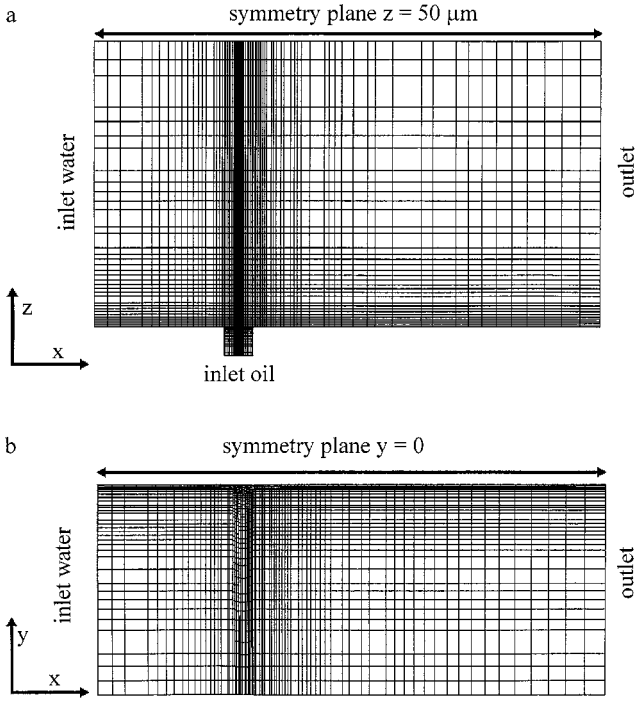

Figure 2. Grid and boundaries of the geometry.

(a) *x-z* plane ($y = 0$); (b) *x-y* plane ($z = 0$). Compare Figure 1b and 1c.

Solver data

The calculation was controlled by the minimum residual value through adaptive time stepping. The values of the parameters are given in Table 2. Unless the parameters are mentioned in this paragraph, the default values of the software package were used.

It took 2320 time steps to calculate the formation of one oil droplet. This required 16 days of CPU time on a dual Pentium-II workstation (operating system Windows NT) with an internal memory of 2*256 MB.

Calculation of the pressure drop over the pore (Δp_p) and the average oil velocity in the pore ($\bar{v}_{p,oil}$).

At several time steps the pressure and the velocity, calculated by CFD, were extracted from the data files. We took the values calculated in the grid cell in the center of the pore at a distance of 0.51 μm below the pore opening. This distance was chosen to avoid effects from the outflow of oil from the pore into the flow channel on the laminar flow in the pore, which was indeed the case for most time steps.

To calculate the total pressure drop over the pore we subtracted the extracted pressure values from the applied absolute pressure (1.3×10^5 Pa) and these values were multiplied by the factor 5.00/4.49, to correct for the total length of the pore. The values for the (maximum) oil velocity, extracted from the data files, were divided by 2 to calculate the average oil velocity in the pore at several time steps (for laminar flow in a cylindrical pore: $v_{\max} = 2\bar{v}_{p,\mathrm{oil}}$).

Table 2. Values of the Solver Parameters used in the Simulation

Solver Parameter	Value
Initial time step	5×10^{-7} s
Min. interval between increments	4 time steps
Time-step multiplying factor*	2
Time-step dividing factor**	1.5
Max. no of iterations per time step	20
Control parameter: min. residual value	5×10^{-12} kg/s

*After four successfully calculated time steps, the time step is multiplied with this factor. Successfully calculated means that the residual value is lower than the given minimum residual value within less than 20 iterations per time step.

**The time step is divided by this factor after a failed calculation; this is the case if the residual value is still higher than the minimum residual value after 20 iterations.

Calculation of the equivalent Laplace pressure

By calculating the oil flux with the average velocity, we calculated the droplet volume increase and the resulting droplet volume at the different time steps [$V_{dr}(t)$]. From the droplet volume we calculated a corresponding equivalent sphere diameter and from that value an equivalent Laplace pressure (Eq. 1)

$$\Delta p_{\mathrm{lapl,eq}}(t) = \frac{4\gamma}{d_{\mathrm{dr,eq}}(t)} = \frac{4\gamma}{\left[6V_{dr}(t)/\pi\right]^{1/3}}, \qquad (1)$$

in which γ is the interfacial-tension coefficient (30 mN/m). This equivalent Laplace pressure is an approximation, because with the CFD calculations it was shown that the droplet is not spherical, but has more curvatures. However, the equivalent Laplace pressure agrees quite well (within 20%) with the pressure drop over the interface in the part of the droplet that is almost spherical.

Results and Discussion

Figure 3a–3d show the velocity profiles of oil and water and the shape of the droplet at four steps in time. Contour lines connect the control volumes in which the volume fraction of oil is equal. The five lines in Figure 3a span the whole oil volume fraction range from 0 to 1 (0.0, 0.25, 0.5, 0.75, and 1.0). In the other figures only the contour line at a volume fraction of 0.5 is shown. Although the interface is rather broad (about five grid cells), we assume that the interfacial-tension force was calculated correctly. The calculation of this force is based on the continuum surface force (CSF) model developed by Brackbill et al. and implemented in CFX 4 by Burt et al. (Brackbill et al., 1992; Burt et al., 1996). The interfacial-tension force is introduced as a body force that is a function of the interfacial-tension coefficient and the curvature. The local curvature is described by the normal vector to the free surface. This vector is given by the gradient of the volume fractions. Both groups validated the model against a series of test cases, including free-surface flows and wall effects (Brackbill et al., 1992; Burt et al., 1996). Therefore, our assumption of the validity of the interfacial-tension force calculations is reasonable.

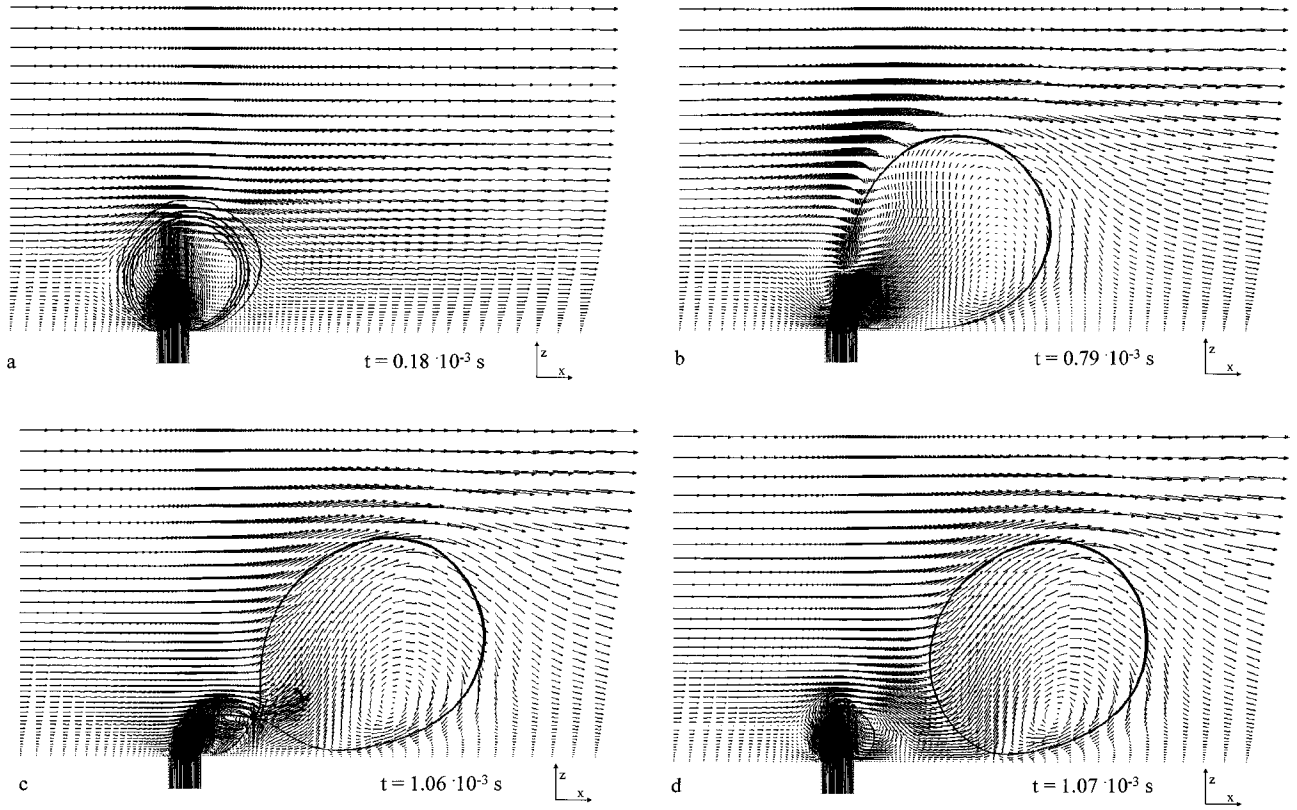

Figure 3. (a–d) Droplet shape (contour lines) and velocities (in m/s, indicated by arrows) of both phases in each grid cell as a function of time, for the plane through the center of the pore (x-z plane; $y = 0$).

Porosity of the membrane

The oil droplet diameter was 33 μm after detachment had taken place (Figure 3d), thus the droplet diameter was about seven times the pore diameter. This ratio is comparable with the experimentally determined droplet/pore diameter ratio of 5 (Katoh et al., 1995). Hence, assuming rigid spherical droplets growing simultaneously, the distance between two pores must be at least six times the pore diameter to avoid contact, and thus avoid coalescence, between two neighboring droplets. But as expected, the droplet is deformed in the direction of flow of the continuous phase, which is shown in Figure 3. Although only one pore was modeled, it can be seen that due to the deformation of the droplet, a space of almost 10 times the pore diameter is needed for unhindered droplet growth in the x-direction. In the y-direction the droplet remained almost spherical throughout the formation process; therefore, the space required in that direction is just seven times the pore diameter. From these data we calculated the maximum porosity of an emulsification membrane. The (surface) porosity is the ratio of the total pore cross-sectional area and the total membrane surface area. Figure 4 shows that the maximum porosity depends on the arrangement of the pores in the membrane. For the so-called uniform grid (Figure 4a), the distance of the pores is 50 μm in the x-direction and 33 μm in the y-direction; as a result, the maximum porosity is 1.2%. With a staggered pore arrangement, the maximum porosity can be slightly higher (Figure 4b): 1.5%.

However, it should be borne in mind that we only simulated the formation of one droplet at a single pore with a constant interfacial tension. First, we expect that droplets growing in a multipore system will have a droplet diameter slightly different from the droplet diameter that was calculated for a single pore, since neighboring droplets disturb the laminar flow profile of the cross-flowing water (Figure 3). A droplet that grows in the ''shade'' of another droplet will experience a different water-flow profile. Second, a constant interfacial tension implies that (dynamical) effects of emulsifiers were not taken into account. Both in a system without emulsifier and in a system with a slow emulsifier (slowly diffusing with respect to the droplet formation time), the interfacial tension will be constant. Addition of a fast emulsifier in a membrane emulsification system will probably affect the droplet shape and the final droplet size. For these reasons, the values for the maximum porosity are only an indication.

Oil flux through the pore

The oil velocity in the pore can be calculated from the pressure drop over the pore (Δp_p) by the Fanning equation (for steady laminar flow in a tubular pipe)

$$\bar{v}_{p,\mathrm{oil}} = \frac{d_p^2 \Delta p_p}{32 \eta_{\mathrm{oil}} l_p}, \qquad (2)$$

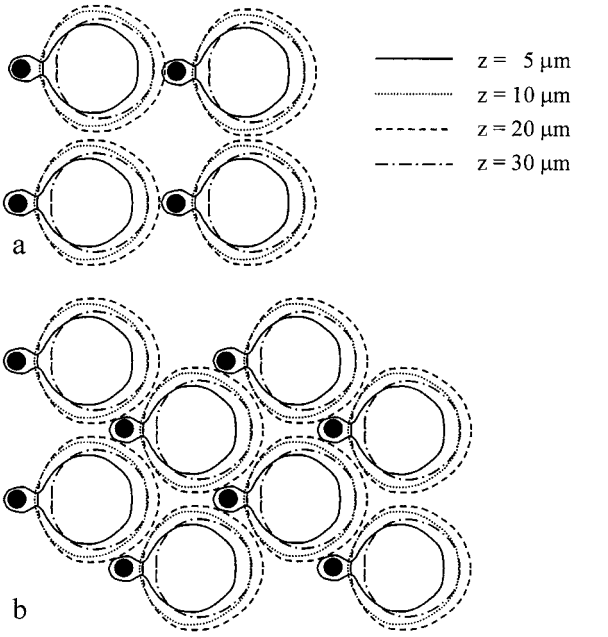

Figure 4. Examples of the arrangement of pores (black dots) in the membrane with contours of the droplet at 4 distances from the membrane at $t = 1.06 \times 10^{-3}$ s.

At $z = 20$ μm, the diameter of the section through the droplet is biggest. (a) uniform arrangement; (b) staggered arrangement.

in which d_p is the pore diameter, η_{oil} the oil viscosity, and l_p the length of the pore. Schröder et al. (1998) reasoned that the velocity of oil in the pore is not constant during the process of droplet formation, because the pressure drop over the pore increases with the size of the droplet. According to them, the total transmembrane pressure can be divided into two parts. One part is the pressure drop over the pore. The other part is the Laplace pressure, being the difference in pressure over the droplet interface, which depends on the curvature of the interface. Because Schröder et al. (1998) assumed a spherical droplet, the Laplace pressure, and thus the pressure drop over the pore, could be calculated. In this section we show that, due to deformation of the droplet, the pressure drop over the pore and the oil velocity in the pore were quite different from those calculated values.

Between 0 and 0.08 ms, the stationary situation is not reached within the iterations per time step, resulting in a decreasing velocity/pressure ratio ($\bar{v}_{p,oil}/\Delta p_p$; Figure 5), but from 0.08 ms onwards, the velocity/pressure ratio is constant; the value follows from the rewritten Fanning equation (Eq. 2)

$$\frac{\bar{v}_{p,oil}}{\Delta p_p} = \frac{d_p^2}{32 \eta_{oil} l_p}$$

$$= \frac{(5 \times 10^{-6})^2}{32 \times 0.003 \times 5 \times 10^{-6}} = 5.2 \times 10^{-5} \text{ m}^2 \cdot \text{s} \cdot \text{kg}^{-1}.$$

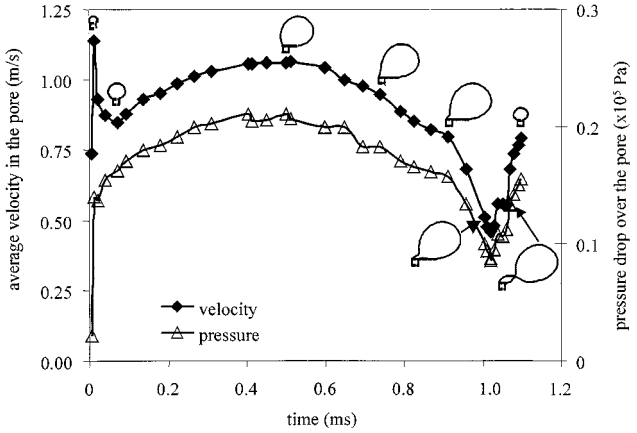

Figure 5. Pressure drop over the pore and average velocity in the pore, both as a function of time; at certain times, the droplet shape is depicted.

In Figure 6 the equivalent Laplace pressure calculated with the equivalent sphere diameter (see section model setup), the pressure drop over the pore, the sum of those two pressures, and the transmembrane pressure are shown at several time steps. The droplet formation can be divided into a few stages. In the first stage, until about 0.5 ms, the droplet remained almost spherical (Figure 5). As a result, the Laplace pressure decreased (compare the equivalent Laplace pressure in Figure 6) and the pressure drop over the pore increased. The sum of the equivalent Laplace pressure and the pressure drop over the pore is almost constant during this stage (Figure 6). In the next stage, the droplet was that much deformed that the oil was hindered from flowing into the droplet and the oil velocity in the pore started to decrease. After 0.9 ms, the velocity decreased sharply, which can be explained by the formation of a neck. Because the neck is only a few micrometers wide, the pressure drop in the neck, between the pore and

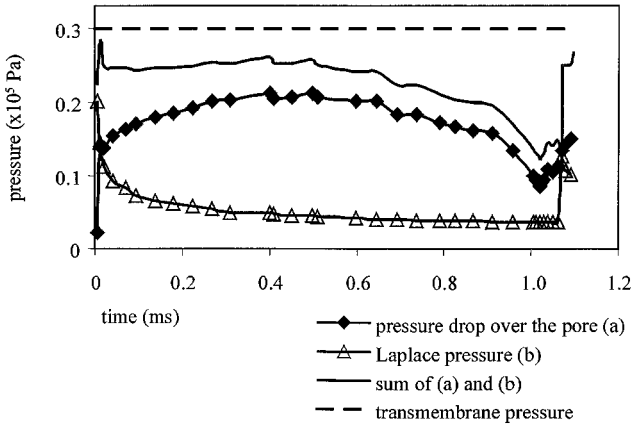

Figure 6. Pressure drop over the pore, calculated from the output data; equivalent Laplace pressure, calculated from the equivalent sphere diameter; sum of both pressures and transmembrane pressure in time.

the droplet, is considerable. This can also be seen in Figure 6: the difference between the sum of the pressures and the transmembrane pressure increases, meaning that there was a resistance against flow somewhere else in the system. At $t =$ 1.0 ms, the neck started to widen, which resulted in a higher oil velocity in the pore. After detachment of the droplet, the pressure drop over the pore and the oil velocity in the pore increased further, because the curvature of the newly forming droplet was less sharp than the curvature of the neck. It is important to note that no satellite droplets were formed and that the Laplace pressure in the new droplet is lower than the critical Laplace pressure at the start of the formation of the first droplet, which was 0.24×10^5 Pa ($= 4\gamma/d_p$). This suggests that as soon as one pore is active, no other pores in the neighborhood will become active, because the driving force (pressure difference over the pore) is higher for the active pore than for a ''starting'' pore. Qualitative observations (not shown) in a microscopic membrane system point in the same direction: only a few pores were active, although they all had the same pore diameter ($d_p = 5$ μm), and thus the same critical pressure. This is in agreement with Schröder (1999); he found that 3–8% of the pores were active at a low transmembrane pressure.

With Figure 6 we show that not only flow in the pore and the Laplace pressure over the interface contribute to the pressure losses in the system, since the sum of these two is never equal to the transmembrane pressure. This is due to viscous dissipation as a result of flow inside the droplet caused by other forces on the droplet (such as drag of the continuous phase). This dissipation term is especially important when the neck is formed, as was explained in the previous paragraph. The pressure drop in the flow channel was negligible.

The time-averaged velocity in the pore ($v_{p,\mathrm{oil}}$) was 0.92 m/s, which is even higher than the average velocity of the water phase. Due to the high velocity, the droplet formation time was short, only 1.06 ms. The high oil flux through the pore was caused by the low oil viscosity ($\eta_{\mathrm{oil}} = 3 \times 10^{-3}$ Pa·s) and the extremely short pore chosen ($l_p = 5$ μm). The value for the formation time (1.06 ms) can therefore not directly be compared with calculated droplet formation times (0.09–1.05 s) from experiments described in the literature because of different conditions (Schröder and Schubert, 1999).

Membrane wetting and fouling

Calculations were performed with a contact angle of 0° for water on the membrane surface, which means that oil will not spread on it. However, in Figure 3b it was shown that the forming oil droplet partly touched the membrane surface, as a result of the deformational forces of the continuous phase on it. In a later stage the membrane was again wetted by water and the droplet completely detached from the membrane surface (although a small part remained at the pore). This formation process indicates that the contact angle with the membrane material should not be too high.

In Figure 7 the pore and part of the flow channel are magnified and oil fractions of 0.5 and 0.99 are given by contour lines. The figure may be an indication of an interesting wetting phenomenon: due to deformation of the droplet in the *x*-direction, water can enter the pore at the other side. This could have practical implications: when doing experiments with proteins as emulsifier, water entering the pore could cause membrane fouling. For example, proteins can stick with their hydrophilic groups to the surface, in this way making the pore hydrophobic and thereby changing the droplet formation process or ultimately even blocking the pore.

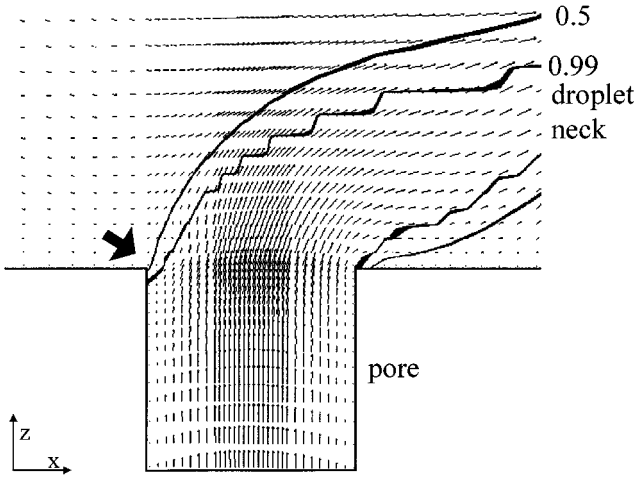

Figure 7. Water entering the pore at $t = 1.05$ ms (indicated with arrow).

Velocity profile (m/s) and contour lines at oil fractions 0.5 and 0.99.

Conclusions

Computational fluid dynamics (CFD) was succesfully used to calculate the shape of a droplet growing at a pore in a laminar cross-flow. These calculations facilitate the design of a membrane, tailor-made for membrane emulsification. For a cylindrical pore ($d_p = 5$ μm), the resulting droplet diameter was 33 μm. However, due to deformation during droplet formation, the pores should be placed more than ten times the pore diameter apart in the direction of flow (*x*-direction), to prevent the coalescence of droplets growing on neighboring pores, under the assumption that the droplets are growing simultaneously. In the *y*-direction only a distance of seven times the pore diameter is needed. The maximum porosity for a membrane with a staggered arrangement of the pores is about 1.5%. Therefore the porosity of a membrane for emulsification has to be low, and should preferably be different in the *x*- and *y*-directions. The velocity of oil through the pore was shown to depend on the shape of the droplet. The velocity sharply decreased at the moment a neck was formed. After detachment of the droplet by further necking, a small droplet remained attached to the pore, which has a Laplace pressure lower than the critical pressure. This will possibly prevent oil from flowing through pores close to a pore that is already active. In case very few pores are active, such that less than 1% of the membrane surface area is used, the porosity of the membrane surface is not relevant any more. Anyhow, coalescence of droplets at the membrane surface will be prevented in that case.

Literature Cited

Brackbill, J. U., D. B. Kothe, and C. Zemach, ''A Continuum Method for Modeling Surface Tension,'' *J. Comput. Phys.*, **100**, 335 (1992).

Burt, D. J., J. W. J. Ferguson, and H. Pordal, ''Numerical Computation of Surface Tension Effects,'' *Proc. ASME*, **3**, 439 (1996)
Joscelyne, S. M., and G. Trägårdh, ''Food Emulsions Using Membrane Emulsification: Conditions for Producing Small Droplets,'' *J. Food Eng.*, **39**, 59 (1999).
Katoh, R., Y. Asano, A. Furuya, and M. Tomita ''Conditions for Preparation of W/O Food Emulsions Using a Membrane Emulsification System,'' *J. Jpn Soc. for Food Sci. and Technol. (Jpn)*, **42**, 548 (1995).
Kawakatsu, T., Y. Kikuchi, and M. Nakajima, ''Regular-Sized Cell Creation in Microchannel Emulsification by Visual Microprocessing Method,'' *J. Amer. Oil Chem. Soc.* **74**, 317 (1997).
Omi, S., ''Preparation of Monodisperse Microspheres Using the Shirasu Porous Glass Emulsification Technique,'' *Colloids Surf. A: Physicochem. Eng. Aspects*, **109**, 97 (1995).
Peng, S. J., and R. A. Williams, ''Controlled Production of Emulsions Using a Crossflow Membrane. Part I: Droplet Formation From a Single Pore,'' *Trans. Inst. Chem. Eng.*, **76**, 894 (1998).
Schröder, V., ''Herstellen von Öl-in-Wasser-emulsionen mit Mikroporösen Membranen,'' PhD Thesis, Technische Hochschule, Karlsruhe, Germany (1999).
Schröder, V., O. Behrend, and H. Schubert, ''Effect of Dynamic Interfacial Tension on the Emulsification Process Using Microporous, Ceramic Membranes,'' *J. Colloid Interface Sci.*, **202**, 334 (1998).
Schröder, V., and H. Schubert, ''Production of Emulsions Using Microporous, Ceramic Membranes,'' *Colloids Surf. A: Physicochem. Eng. Aspects*, **152**, 103 (1999).

Manuscript received March 27, 2000, and revision received Oct. 5, 2000.